

PHYSICAL AND MATHEMATICAL MODELLING INVESTIGATIONS OF THE MECHANISMS OF SPLASH GENERATION IN BATH SMELTING FURNACES

Yuhua PAN¹ and David LANGBERG²

¹ CSIRO Minerals, Clayton, Victoria 3169, AUSTRALIA
Corresponding author, E-mail address: Yuhua.Pan@csiro.au

² Formerly CSIRO Minerals, Clayton, Victoria 3169, AUSTRALIA

ABSTRACT

The behaviour of large gas bubbles in a liquid bath and the mechanisms of splash generation due to gas bubble rupture in high-intensity bath smelting furnaces were investigated by means of physical and mathematical (CFD) modelling techniques. In the physical modelling work, a two-dimensional Perspex model of the pilot plant furnace at CSIRO Minerals was established in the laboratory. An aqueous glycerol solution was used to simulate liquid slag. Air was injected via a submerged lance into the liquid bath and the bubble behaviour and the resultant splashing phenomena were observed and recorded with a high-speed video camera. In the mathematical modelling work, a two-dimensional CFD model was developed to simulate the free surface flows due to motion and deformation of large gas bubbles in the liquid bath and rupture of the bubbles at the bath free surface. It was concluded from these modelling investigations that the splashes generated in these furnaces are mainly caused by the rupture of fast rising large gas bubbles. The acceleration of the bubbles into the preceding bubbles and the rupture of the coalescent bubbles at the bath surface contribute significantly to splash generation.

Keywords: Physical modelling, mathematical modelling, CFD, free surface flow, bubble and splash.

NOMENCLATURE

S_ϕ	source term in governing transport equations
t	time
\mathbf{u}	velocity vector
α	scalar variable for tracking liquid-gas interface
ϕ	general variable in governing transport equations
μ_l	dynamic viscosity
μ_t	turbulent viscosity
ρ	density
σ	surface tension coefficient

INTRODUCTION

Bath smelting reactors such as the Siros melt, Ausmelt and Isasmelt furnaces are examples of modern, high-intensity pyrometallurgical reactors characterised by high-productivity and good feedstock flexibility. Submerged injection of gases at high flowrates produces rapid mixing in the bath ensuring fast chemical reactions and bath homogenisation. However, the strong dynamic interactions between the injected gas and the liquid bath lead to intensive splashing. This can be a problem if the splashes become so heavy that they form accretions on the

furnace wall and roof and in the gas offtake duct. This can cause unscheduled shutdowns which adversely affect productivity. In addition, the splashes can cause safety problems. Therefore, in order to find effective means to control the splash intensity in Siros melt and other bath smelting furnaces, the present work was carried out to investigate the behaviour of large gas bubbles in slag baths and the mechanisms of splash generation in such furnaces by using both physical and mathematical (CFD) modelling techniques.

Splashing phenomena due to submerged injection of gas into a liquid bath has been extensively studied. Past investigations of such phenomena have been well reviewed by Liow (1992), Cullinan (1993) and Guerra (1995). Among the past studies, the splashes caused by gas bubble rupture received broad attention and were investigated more extensively. However, as pointed out by Liow et al. (1996), the majority of the previous work was made only on small bubbles (less than 10 mm in diameter or equivalent). In Siros melt furnaces, for example, the size of the bubbles formed in the liquid bath can be expected to be very large (above 50 mm in diameter). This situation requires new interpretations of the mechanisms of splash generation in such furnaces. Therefore, since mid-1980s, extensive physical modelling studies on the splash generation in Siros melt furnaces were carried out at The University of Melbourne and at CSIRO Minerals (Liow et al., 1995; Liow et al., 1996; Nilmani and Conochie, 1986; Koh and Batterham, 1989). Besides the physical modelling investigations, a number of mathematical modelling studies on the fluid flow phenomena in Siros melt furnaces were also carried out by means of CFD simulation techniques (Schwarz and Koh, 1986; Liovic et al., 1999; Liovic et al., 2002).

However, the published research results reveal that the behaviour of large gas bubbles at the liquid bath free surface and the mechanisms of resultant splash generation in bath smelting furnaces are yet to be fully understood and more relevant experimental data are necessary to verify the CFD model simulations. Therefore, the major objective of this work is to apply both physical and CFD modelling techniques to investigate the large gas bubble behaviour and the mechanisms of splash generation in bath smelting furnaces.

PHYSICAL MODELLING

Figure 1 schematically illustrates a two-dimensional (2D) slice physical model, made of Perspex, of the 300 kg pilot furnace in the laboratory of CSIRO Minerals. Water and 91.5% (wt./wt.) aqueous glycerol solution (aqueous

glycerol for short) were respectively used as the modelling media, with the latter simulating liquid slag.

One set of the experiments was carried out to observe the gas bubble motion and rupture as they cross the liquid bath surface, by using a high-speed video camera. In these experiments, air was injected at different flowrates, ranging from 12 to 120 Nm³/h, into an aqueous glycerol bath held in the model. The height of the liquid bath was 30 cm and the lance immersion depth was 15 cm measured from the quiescent bath free surface (cf., Figure 1).

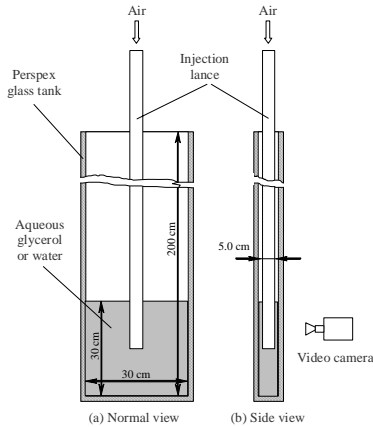


Figure 1: Schematic diagram of a two-dimensional physical model set-up of the CSIRO pilot plant furnace.

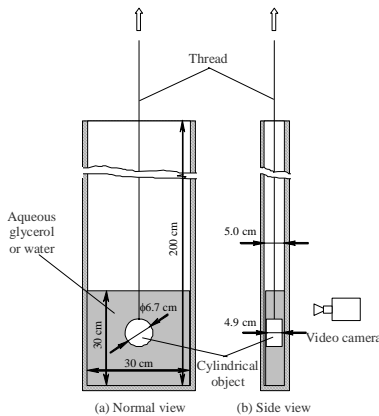


Figure 2: Schematic diagram of two-dimensional physical model set-up for liquid film thickness measurement.

Another set of the experiments was performed on the physical model set-up shown by Figure 2 to measure the liquid film thickness above a solid object approaching the liquid surface for validation of the CFD model developed in the present work. In this model set-up, as compared with Figure 1, the injection lance was replaced with a hanging solid cylindrical object. This object was immersed into the liquid bath and then lifted out of the bath at different velocities, simulating flotation of a “rigid bubble” in the liquid bath. In each experiment the object was lifted manually at different velocities out of the liquid bath by using a thread mounted onto the object. The experiments were performed on both an aqueous glycerol bath and a water bath. As the object rose across the bath surface, a liquid film remaining on the leading cylindrical surface of the object was recorded by using a high-speed video camera. The thickness of this liquid film was measured from the recorded video images and then, as a

means of model validation, compared with the CFD model predictions.

MATHEMATICAL MODELLING

Governing Equations

The free surface flow phenomena due to motion of large gas bubbles in a liquid bath in the above-mentioned physical model were mathematically simulated by using a commercial CFD modelling package PHOENICS-3.5 (CHAM Ltd., 2002) and a transient 2D numerical model was developed. In this modelling work, an approach called the Scalar-Equation-Method (SEM) in-built with PHOENICS was applied to simulate the flow phenomena of interest. In this mathematical approach, a set of governing partial differential equations are solved, which, in a generalised vector notation form, reads

$$\frac{\partial(\rho\phi)}{\partial t} + \nabla \cdot (\rho\phi\mathbf{u}) = \nabla \cdot [(\mu_l + \mu_t)\nabla\phi] + S_\phi \quad (1)$$

where ϕ is a general variable standing for unity (continuity equation), velocity components (momentum equations), turbulence kinetic energy and the dissipation rate of the turbulence kinetic energy (k- ϵ turbulence equations).

In SEM simulation of free surface flows, the following equation is derived from Eq. (1), by setting ϕ equal to a dimensionless scalar variable α and neglecting the diffusion and source terms, for tracking the location of the gas-liquid interface (i.e., free surface):

$$\frac{\partial\alpha}{\partial t} + \nabla \cdot (\alpha\mathbf{u}) = 0 \quad (2)$$

where α , having a numerical range between 0 and 1, is used as a fluid marker. By convention, $\alpha = 0$ refers to the lighter fluid (gas); $\alpha = 1$ to the heavier fluid (liquid); and $0 < \alpha < 1$ marks the position of the gas-liquid interface.

The governing equations (1) and (2) constricted by proper initial and boundary conditions described below were solved numerically. To minimise numerical diffusion when tracking the gas-liquid interface, which is physically a sharp interface, a special numerical differencing scheme called the *van Leer Scheme* was implemented (CHAM Ltd., 2002).

In the present CFD model, the liquid phase refers to aqueous glycerol or water while the gas phase refers to air, both at room temperature. Table 1 gives the physical properties of these materials used in the CFD model.

Computation domain

Figure 3 shows the computation domain defined according to the dimensions of the physical model shown in Figure 1 or Figure 2. In order to save computer storage and computation time, the computation domain was limited in its vertical extent (50 cm), instead of the actual height (200 cm) of the physical model.

Material	Density (kg/m ³)	Dynamic viscosity (Pa.s)
Aqueous glycerol ¹	1240	0.35
Water ²	998	0.001
Air ³	1.19	1.836 × 10 ⁻⁵

¹<http://www.dow.com/glycerine/resources/physicalprop.htm>

²http://www.engineeringtoolbox.com/water-thermal-properties-d_162.html

³http://www.engineeringtoolbox.com/air-properties-d_156.html

Table 1: Physical properties used in the CFD model

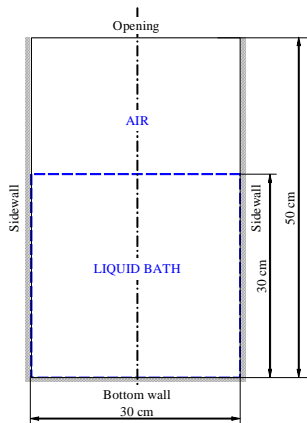


Figure 3: Two-dimensional computation domain defined in the CFD model (cf., Figures 1 and 2).

Initial and Boundary Conditions

The developed CFD model is transient and thus, as an initial condition, all computations were started with a quiescent liquid bath. The injection lance and bubble growth at its tip were neglected so that it was assumed that a gas bubble with a certain initial size (diameter) can suddenly appear in the liquid bath. As boundary conditions (cf., Figure 3), all boundary walls were considered non-slip to the fluids and the top boundary of the computation domain was set open to the atmosphere, to which a fixed pressure condition was applied.

In addition to the assumptions mentioned above, one major assumption made in the present CFD model was that, since we only focused on gas bubbles with fairly large sizes (diameter ≥ 80 mm), the effect of liquid surface tension force would be very small compared to fluid inertia and gravity and thus neglected.

Numerical Simulations

In this work, the CFD model was first applied to simulate the motion of a “rigid bubble” (solid object) in an aqueous glycerol bath and a water bath, respectively, held in the physical model set-up shown in Figure 2. In these simulations the thickness of the liquid film formed on the leading surface of the cylindrical object was predicted and, as a means of model validation, compared with those measured from the video images recorded during the physical modelling experiments. Then, by changing the “rigid bubble” into a deformable gas bubble, the CFD model was applied to simulate the motion of large gas bubbles in an aqueous glycerol bath held in the physical model set-up shown in Figure 1. In these CFD simulations, the behaviours of a single bubble and two bubbles in the liquid bath were predicted, respectively. As an important result, the variations of the dome film

thickness as the bubbles rise across the bath surface were predicted, because such knowledge is helpful for in-depth understanding on the mechanisms of splash generation due to gas injection in bath smelting furnaces.

RESULTS AND DISCUSSION

Validation of CFD Model

Figure 4 shows a time series of video images of a cylindrical object rising out of an aqueous glycerol bath in comparison with the corresponding results predicted by the CFD model. In the CFD model simulated images, the red colour region stands for the liquid phase while the blue colour region for the gas phase. The border between the two-coloured regions stands for the free surface. It can be seen from this figure that the CFD model predicted very similar free surface profiles to those observed from the physical model. Figure 5 gives the CFD model predicted liquid film thickness at the apex of the cylindrical surface in comparison with those measured at the corresponding location from the physical model for different rising (lifting) velocities. This figure clearly demonstrates that the CFD model can provide rather consistent predictions on the liquid film thickness with those observed from the physical model. These results provide a level of confidence to apply the CFD model to simulate the behaviours of large gas bubbles in bath smelting furnaces.

Behaviour of Single Large Bubble in Liquid Bath

Figure 6 shows a time series of the video images for an experimental case in which a large gas bubble (diameter = 160 mm) is moving in an aqueous glycerol bath. This figure also includes roughly corresponding images of this process simulated by the CFD model. It can be seen that the bubble deformation simulated by the CFD model is quite similar to that observed from the physical model.

It should be noted here that the time lapses of the images predicted by the CFD model do not correspond to those observed from the physical model. This is because, as an initial condition, the CFD model simulation started with a quiescent bath whereas in the physical model the video recordings were taken from an already agitated bath (by the preceding bubbles). Therefore, the bubble simulated by the CFD model floated more slowly than that in the physical model.

Behaviour of Two Large Bubbles in Liquid Bath

Figure 7 illustrates a time series of CFD model predicted images depicting the interesting behaviour of two 80-mm bubbles initially generated at different heights in an aqueous glycerol bath. Soon after the two bubbles are formed, the lower bubble quickly accelerates into the upper bubble. Moreover, the dome film of the second bubble breaks up forming jets inside the first bubble. As the time lapses, the two bubbles merge together forming a single large bubble. This coalescent bubble finally bursts, creating large splashes.

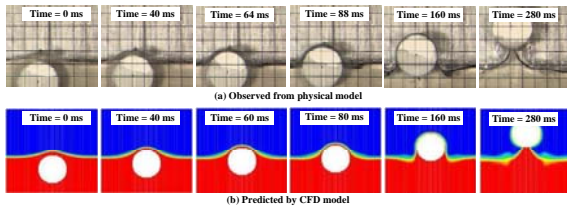


Figure 4: Comparison between the motion of a cylindrical object rising out of an aqueous glycerol bath in the physical model (cf., Figure 2) and that simulated by the CFD Model (object rising velocity = 0.296 m/s).

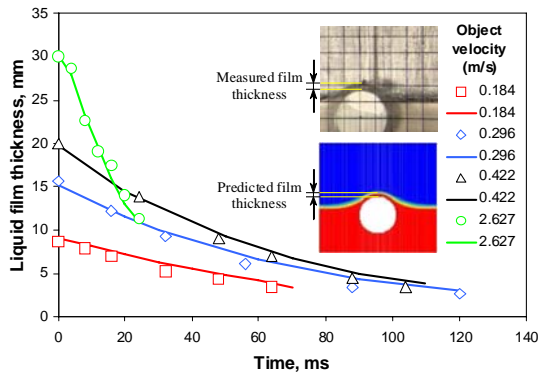


Figure 5: Comparison between variations of the liquid film thickness measured on the solid object top surface in the physical model (cf., Figure 2) for different object rising velocities and those predicted by the CFD model. (Symbols stand for physical model measurements and curves for CFD model predictions.)

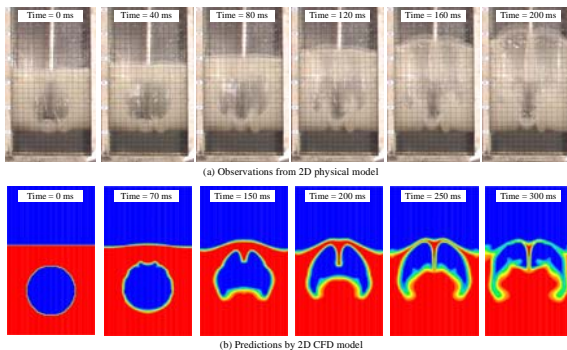


Figure 6: CFD model predicted behaviour of a 160-mm gas bubble in an aqueous glycerol bath in comparison with observations from the physical model (cf., Figure 1).

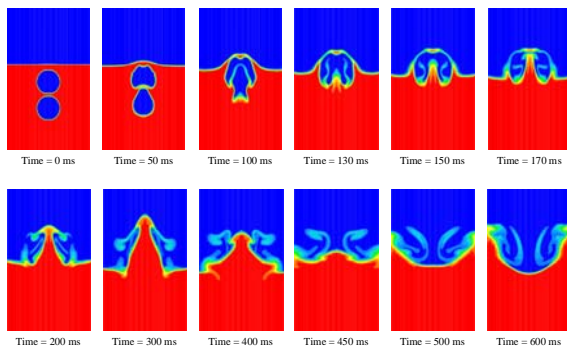


Figure 7: CFD model predicted behaviour of two 80-mm gas bubbles in an aqueous glycerol bath.

More interestingly, upon breaking-up, the bottom of the coalescent bubble develops into a strong liquid jet (Rayleigh jet). This jet can rise to a height almost equal to the original depth of the bath. Thus, it can be anticipated that the splashes generated by this jet disintegration would possess very high kinetic energy and thus can fly over a great distance. After the jet reaches a maximum height, it starts to collapse. The downward movement of the jet drives the liquid to the periphery of the bath forming a concave free surface with a large potential energy. After that, driven by this potential energy, the bath surface turns convex and concave periodically inducing a wave-like bath slopping. This result demonstrates that an ensemble of large gas bubbles in a liquid bath can induce much intensive agitation of the bath than do bubbles acting individually.

The liquid jet formation due to acceleration of a bubble into the preceding bubble predicted by the present CFD model shown in Figure 7 is verified by the experimental observations made by Liow et al. (1996) shown in Figure 8. This result further supports the validity of the CFD model in simulating free surface flows induced by the motion of large gas bubbles.

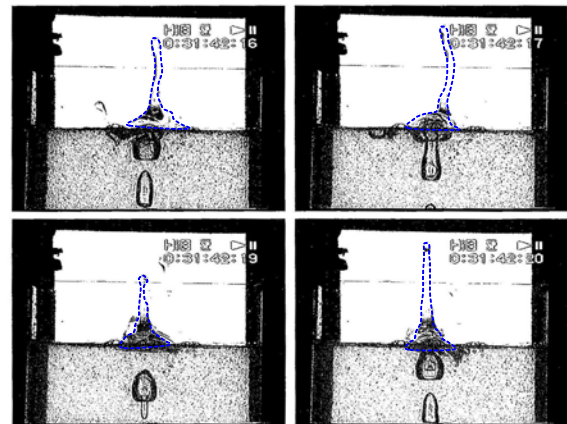


Figure 8: Observed liquid jets formed by two interacting bubbles in a glycerol bath at an injection depth of 0.1 m and a gas flow rate of 13.4 litres/minute, adapted from Liow et al. (1996). (For clarity, the outline of the liquid jets is marked with dashed curves by the present authors.)

Figures 4 to 7 also indicate that the liquid film thickness is not uniform, and the thinnest part of the film would more likely be the weakest point at which rupture of the film takes place. Therefore, it is of primary interest to apply the physical and CFD models to predict influences of factors on film thickness variations at the bath surface.

Influence of Bubble Rising Velocity on Splash Generation

Figure 5 shows the influence of the rising velocity of the solid object in an aqueous glycerol bath on the variation of the liquid film thickness with time. Initially, a higher rising velocity leads to a thicker liquid film and vice versa. This is because, if the object rises slowly toward the bath surface the liquid in front of it has enough time to drain away, leaving a thin liquid layer above the object. As the object rises across the bath surface, the liquid film drains naturally and thus its thickness decreases slowly. Conversely, if the object rises rapidly, the liquid trapped in front of it doesn't have time to give way, forming a

thick initial liquid layer. However, as the object rises across the bath surface, the liquid drains out quickly as if it is “squeezed” out of the film.

Influence of Bubble Size on Splash Generation

Figure 9 illustrates the CFD model predicted variations of the minimum film thickness with time for two gas bubbles of different sizes (80 and 160 mm in diameter) each moving in an aqueous glycerol bath. It can be seen from this figure that initially the 160-mm bubble possesses a thicker film than that of the 80-mm bubble. However, the minimum film thickness of the 160-mm bubble decreases more rapidly with time than the 80-mm bubble as they rise across the bath surface. This is because the larger bubble has a higher rising velocity and hence a thicker dome film. This result is consistent with that shown in Figure 5 for a “rigid bubble”.

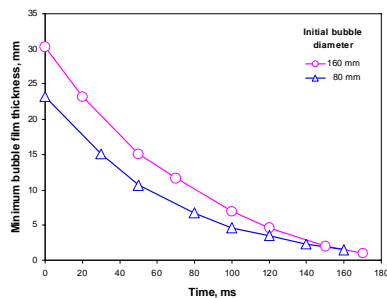


Figure 9: CFD model predicted variations in minimum film thickness of two different size gas bubbles in aqueous glycerol bath with time.

Furthermore, the CFD modelling results also indicate that a large bubble has a more uneven film layer than a smaller one. Thus, while the film of the larger bubble is generally thicker than that of the smaller bubble, during rising across the bath surface the larger bubble can have a part of film even thinner than that of the smaller bubble. Since this part of bubble film could be the weakest point, the rupture of a large bubble can produce larger size splashes. Therefore, the dome film of a large bubble is more dynamic than that of a small bubble and, consequently, generates more splashes upon rupture at the bath surface.

The results shown in Figures 5 and 9 can be used to interpret in part the mechanisms of splashing phenomena in bath smelting furnaces. A high gas injection flowrate generally produce large gas bubbles that rise rapidly in the slag bath. Upon reaching the bath surface, the thickness of the bubble dome film is thick but decreases quickly as the bubbles rise out of the bath. If the gas injection flowrate is high enough, the liquid trapped in front of the bubble doesn’t drain out naturally but is “squeezed” out by combined forces of the pressure inside the bubble (due to buoyancy and surface tension) acting on the inner surface of the bubble film and the form (friction) pressure (due to bubble motion) and the surface tension acting on the outer surface of the bubble film. These understandings may explain the fact that high gas injection flowrates generally result in more intensive splashes in bath smelting furnaces and vice versa. Therefore, one way to control the splash intensity at high gas injection flowrates is to produce smaller bubbles. This understanding is supported by the findings of Nilmani and Conochie (1986) in their experimental studies showing that a swirled lance induces

less splashes than a plain straight pipe lance, because the former lance produces relatively smaller bubbles than the latter does.

Influence of Viscosity on Splash Generation

By using the modelling results obtained from the physical model set-up shown in Figure 2, one can also investigate the influence of liquid viscosity on splash generation. Figure 10 gives the measured initial liquid film thickness as a function of the object rising velocity, when the object is lifted out of an aqueous glycerol bath and a water bath, respectively. This figure depicts that the liquid film initially formed in front of the object in the aqueous glycerol bath is thicker than that in the water bath. This is because the aqueous glycerol has a much higher dynamic viscosity (0.35 Pa·s) than the water (0.001 Pa·s), so that the aqueous glycerol drains slowly in front of the object, leaving a thick layer of liquid film when the object approaches the bath surface. This result implies that in bath smelting furnaces high slag viscosity could result in a thicker initial bubble film that eventually breaks up into more intensive splashes and vice versa.

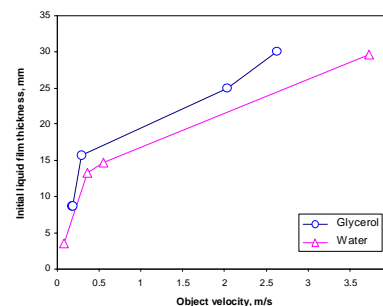


Figure 10: Measured liquid film thicknesses in aqueous glycerol and water baths in physical model for different object rising velocities.

Figure 11 shows both measured and predicted variations of liquid film thickness with time in aqueous glycerol and water baths. This figure indicates that, at similar object rising velocities, the aqueous glycerol film is thicker than the water film and both thicknesses decrease at nearly the same rate. Thus, we can use this result to infer that in bath smelting furnaces, under the same gas injection conditions, a more viscous slag forms a thicker bubble film and hence generates more splashes.

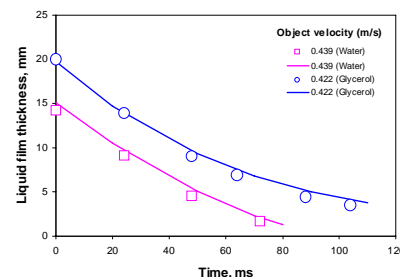


Figure 11: Measured and predicted variations of liquid film thickness with time in aqueous glycerol and water baths. (Symbols stand for physical model measurements and curves for CFD model predictions.)

Validity of Model Assumption

Among the assumptions made in the present CFD model, the biggest uncertainty that may affect the model validity

could be the assumption of neglecting the effect of liquid surface tension. This assumption was made based on the fact that we mainly focus on large bubbles. This emphasis means that the curvature of the gas-liquid interface is sufficiently small resulting in negligible surface tension effects compared to the fluid inertia.

To verify this assumption, the surface tension effect has to be considered in the CFD model. Since the SEM method in-built with the CFD modelling package PHOENICS-3.5 and used in this work doesn't take the surface tension force into account, another commercial CFD modelling package ANSYS CFX 11 (ANSYS Inc., 2009) was used to simulate the same phenomenon shown in Figure 6(a), with and without considering the surface tension coefficient of the aqueous glycerol (0.064 N/m). Figure 12 gives the CFD modelling results showing that very similar free surface profiles are predicted for $\sigma = 0.064$ N/m and $\sigma = 0$ N/m, confirming that the surface tension effect indeed can be neglected for simulating large bubble motion in an aqueous glycerol bath.

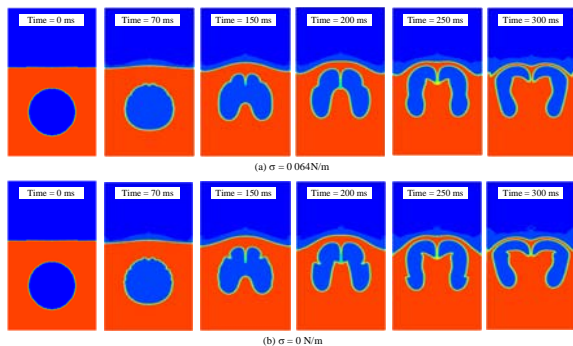


Figure 12: Comparison between the ANSYS CFX simulation results on the motion of a 160-mm gas bubble in an aqueous glycerol bath in the physical model (shown in Figure 1) with and without considering the surface tension effect.

CONCLUSIONS

Based on the present physical and CFD modelling results, the following conclusions can be drawn:

- A faster rising gas bubble in a liquid bath has a thicker film whose thickness decreases quickly and unevenly at the bath surface and eventually breaks up into more splashes, and vice versa.
- A larger gas bubble floats faster in a liquid bath forming a thicker film that eventually breaks up into big splashes.
- Acceleration of a bubble into a preceding bubble can produce a strong liquid jet. Collapse of this liquid jet induces heavy bath slopping leading to intensive splashing.
- A more viscous liquid forms a thicker bubble film that can break up into more splashes.
- In bath smelting furnaces, large gas injection flowrates produce big bubbles that have high rising velocities, forming thick bubble films and hence generating more splashes.
- The splash intensity in bath smelting furnaces could be controlled by i) producing small and discrete bubbles, ii) avoiding bubble coalescence, and iii) decreasing slag melt viscosity by heating to enough high temperatures.

ACKNOWLEDGMENT

The authors would like to acknowledge the financial support for this research work from CSIRO Minerals. Thanks are also presented to Mr. Justen Bremmell for performing physical modelling experiments and to Mr. Steve Sanetsis for taking and processing video recordings.

REFERENCES

- ANSYS Inc., 2009, ANSYS CFX User Manual, Release 12.0.
- CHAM Ltd., 2002, *PHOENICS Encyc.*, London, UK, http://www.cham.co.uk/phoenics/d_polis/d_lecs/semlec.htm
- CULLINAN, V.J., (1993), "Splashing due to Gas Injection", *Master Thesis*, G. K. Williams Cooperative Research Centre for Extractive Metallurgy, The University of Melbourne, Australia.
- GUERRA, A.E., (1995), "Splash in Metallurgical Vessels", *Document number: LITIN5.DOC271195*, G. K. Williams Cooperative Research Centre for Extractive Metallurgy, The University of Melbourne, Australia.
- KOH, P.T.L. and BATTERHAM, R.J., (1989), "Liquid Splashes from Submerged Gas Injection", *Chem. Eng. Res. Des.*, **67**, 211 - 215.
- LIOVIC, P.; RUDMAN, M. and LIOW, J.L., (1999), "Numerical Modelling of Free Surface Flows in Metallurgical Vessels", *Proc. Second Int. Conf. CFD in Minerals and Process Ind.*, CSIRO, Melbourne Australia, December, 255 - 260.
- LIOVIC, P.; RUDMAN, M. and LIOW, J.L., (2002), "Numerical Modelling of Free Surface Flows in Metallurgical Vessels", *J. App. Math. Modelling*, **26**, 113 - 140.
- LIOW, J.L., (1992), "Interfacial Phenomena", *Mervyn Willis Symposium and Smelting & Refining Course*, G. K. Williams Cooperative Centre for Extractive Metallurgy, University of Melbourne, Australia, July, 32:1-32:15.
- LIOW, J.L.; MORTON, D.E.; GUERRA, A.E. and GRAY, N.B., (1996), "Dynamics of Splash Formation in Gas Injected Systems", *Proc. Howard Wornor Int. Sym. Inj. Pyromet.*, Edited by Madhu Nilmani and Theo Lehner, Melbourne, Australia, July, 175-190.
- NILMANI, M. AND CONOCHIE, D.S., (1986), "Gas Dispersion with Swirled Lances", *Proc. SCANINJECT IV*, MEFOS, Lulea, Sweden, June, 7:1 - 7:19.
- SCHWARZ, M.P. and KOH, P.T.L., (1986), "Numerical Modelling of Bath Mixing by Swirled Gas Injection", *Proc. SCANINJECT IV*, MEFOS, Lulea, Sweden, June, 6:1 - 6:17.